UNIVERSITY of York

This is a repository copy of *Theoretical and Experimental Study on the Reaction of tert-Butylamine with OH Radicals in the Atmosphere*.

White Rose Research Online URL for this paper:
http://eprints.whiterose.ac.uk/131537/

Version: Accepted Version

Article:
Tan, Jun-Wen, Zhu, Liang, Mikoviny, Tomáš et al. (11 more authors) (2018) Theoretical and Experimental Study on the Reaction of tert-Butylamine with OH Radicals in the Atmosphere. Journal of Physical Chemistry A. pp. 4470-4480. ISSN 1089-5639

https://doi.org/10.1021/acs.jpca.8b01862

Reuse
Items deposited in White Rose Research Online are protected by copyright, with all rights reserved unless indicated otherwise. They may be downloaded and/or printed for private study, or other acts as permitted by national copyright laws. The publisher or other rights holders may allow further reproduction and re-use of the full text version. This is indicated by the licence information on the White Rose Research Online record for the item.

Takedown
If you consider content in White Rose Research Online to be in breach of UK law, please notify us by emailing eprints@whiterose.ac.uk including the URL of the record and the reason for the withdrawal request.

White Rose university consortium
Universities of Leeds, Sheffield & York

eprints@whiterose.ac.uk
https://eprints.whiterose.ac.uk/

Theoretical and Experimental Study on the Reaction of *tert*-Butylamine with OH Radicals in the Atmosphere

Wen Tan[1§], Liang Zhu[1§], Tomáš Mikoviny[1], Claus J. Nielsen[1,2], Armin Wisthaler[1,3,*], Philipp Eichler[3], Markus Müller[3], Barbara D´Anna[4], Naomi J. Farren[5], Jacqueline F. Hamilton[5], Jan B. C. Pettersson[6], Mattias Hallquist[6], Simen Antonsen[7], Yngve Stenstrøm[7]

1 Department of Chemistry, University of Oslo, P.O. Box 1033 Blindern, 0315 Oslo, Norway
2 Centre for Theoretical and Computational Chemistry, Department of Chemistry, University of Oslo, P.O. Box 1033 Blindern, 0315 Oslo, Norway
3 Institute of Ion Physics and Applied Physics, University of Innsbruck, 6020 Innsbruck, Austria
4 IRCELYON, CNRS, University of Lyon, 69626 Villeurbanne, France
5 Wolfson Atmospheric Chemistry Laboratories, Department of Chemistry, University of York, York YO10 5DD, United Kingdom
6 University of Gothenburg, Department of Chemistry and Molecular Biology, Atmospheric Science, 41296 Gothenburg, Sweden
7 Faculty of Chemistry, Biotechnology and Food Science, Norwegian University of Life Sciences, P.O. Box 5003, 1432 Ås, Norway

[§] These authors contributed equally to this manuscript.

Corresponding author

* armin.wisthaler@kjemi.uio.no. Phone: +47-228-59139. Fax: +47-228-55441

Abstract

The OH-initiated atmospheric degradation of *tert*-butylamine (tBA), $(CH_3)_3CNH_2$, was investigated in a detailed quantum chemistry study and in laboratory experiments at the European Photoreactor (EUPHORE) in Spain. The reaction was found to mainly proceed via hydrogen abstraction from the amino group, which in the presence of nitrogen oxides (NO_x), generates *tert*-butylnitramine, $(CH_3)_3CNHNO_2$, and acetone as the main reaction products. Acetone is formed via the reaction of *tert*-butylnitrosamine, $(CH_3)_3CNHNO$, and/or its isomer *tert*-butylhydroxydiazene, $(CH_3)_3CN{=}NOH$, with OH radicals, which yield nitrous oxide (N_2O) and the $(CH_3)_3\dot{C}$ radical. The latter is converted to acetone and formaldehyde. Minor predicted and observed reaction products include formaldehyde, 2-methylpropene, acetamide and propan-2-imine. The reaction in the EUPHORE chamber was accompanied by strong particle formation which was induced by an acid-base reaction between photochemically formed nitric acid and the reagent amine. The *tert*-butylaminium nitrate salt was found to be of low volatility, with a vapour pressure of 5.1×10^{-6} Pa at 298 K. The rate of reaction between *tert*-butylamine and OH radicals was measured to be $8.4 (\pm 1.7) \times 10^{-12}$ cm^3 $molecule^{-1}$ s^{-1} at 305 ± 2 K and 1015 ± 1 hPa.

1 INTRODUCTION

Amine-based post-combustion carbon capture (PCCC) is a technically and economically viable solution for decarbonizing industrial point sources. While it is possible to remove more than 90% of the carbon dioxide (CO_2) from industrial flue gases using amine solvent blends, small amounts of amines are usually released into the atmosphere from PCCC facilities. Once airborne, these amines will undergo photo-oxidation resulting in the formation of imines, amides, nitrosamines, nitramines and other degradation products.[1,2] In addition, amines will contribute to aerosol formation via acid-base reactions and contribute to particle growth in the atmosphere.[3,4,5,6,]

The atmospheric degradation products of amines, both in the gaseous and particulate state, may pose a risk to human health and the environment.[7] Compounds of particular concern are the nitrosamines and nitramines, which are known or potential carcinogens.[8] The Norwegian Institute for Public Health (NIPH) recommends the total amount of nitrosamines and nitramines in the atmosphere not to exceed 0.3 ng m^{-3}.[9] For assessing the population's exposure to amine degradation products in the vicinity of PCCC facilities, the kinetics and products of atmospheric amine degradation must be known.

The photo-oxidation of 2-aminoethanol (MEA, $NH_2CH_2CH_2OH$), a benchmark compound in PCCC, has been systematically investigated in computational and experimental studies.[5,10,11,12] A relatively high energy penalty and fast solvent degradation do, however, call for the use of alternative solvents.[13] Sterically hindered amines,[14] such as 2-amino-2-methyl-1-propanol (AMP, $(CH_3)_2C(NH_2)CH_2OH$), are prominent candidates due to their higher CO_2 loading capacity, lower carbamate stability and reduced susceptibility towards solvent degradation.[15,16] While the thermal and oxidative degradation of AMP in the solvent have been well studied,[17,18] its atmospheric degradation remains poorly constrained.[10] The presence of the OH substituent complicates both the theoretical and experimental analysis of its atmospheric degradation processes. Herein we thus investigate the atmospheric fate of *tert*-butylamine (tBA), $(CH_3)_3CNH_2$, which resembles the AMP molecule but lacks the OH substituent. We present the first mechanistic insights into the atmospheric degradation of an amine in which the primary amino group is attached to a tertiary carbon. Our work will serve as a basis for future work on the atmospheric degradation of AMP and other sterically hindered amines.

2 MATERIALS AND METHODS

2.1 Computational methods

Quantum Chemical Calculations. Stationary points on the potential energy surface for the reaction of OH with tBA were characterized in M06-2X[19] and MP2[20] calculations employing the aug-cc-pVDZ and aug-cc-pVTZ[21,22] basis sets. Pre and post reaction complexes were located by following the intrinsic reaction coordinate (IRC)[23,24,25] from the saddle points. The energies of the stationary points were then improved with explicitly correlated coupled cluster singles and doubles calculations with perturbative triples scaled as recommended in the Molpro manual, denoted CCSD(T*)-F12a.[26,27] Reaction enthalpies and proton affinities were calculated using the G4 model chemistry.[28] Dipole moments and isotropic polarizabilities used for predicting ion-molecule reaction rate coefficients[29] and instrumental response factors were obtained in B3LYP/aug-cc-pVDZ and M06-2X/aug-cc-pVDZ

calculations. The coupled cluster calculations were performed in Molpro 2012.1[30,31] whereas the DFT, G4 and MP2 calculations were performed in Gaussian 09.[32]

Kinetics calculations. Master equation calculations were carried out using the program MESMER 3.0 (Master Equation Solver for Multi-Energy-well Reactions)[33] for simulating the kinetics of the OH radical reactions with tBA and the branching in consecutive reactions at atmospheric conditions. The required input parameters for molecules, intermediate species and products were obtained from a*b initio* calculations. Phenomenological rate coefficients were extracted from the chemically significant eigenvalues using a procedure similar to that described by Bartis and Widom.[34,35] Lennard-Jones parameters for the various molecular species were approximated with values for the hydrocarbon of similar size and shape.[36] For N_2 and O_2 we used $\sigma(N_2)$ = 3.74 Å, ε/k (N_2) = 82 K, $\sigma(O_2)$ = 3.48 Å and $\varepsilon/k_B(O_2)$ = 103 K.[36] The energy transfer in collisions with N_2 and O_2, $\langle\Delta E_{down}\rangle$, was set to 250 cm^{-1}. Variation of these parameters resulted in only minor differences in the calculations. Spin-orbit coupling in the OH radical (139.7 cm^{-1})[37] was included in the kinetic model by lowering the energy of the OH radical with half of the splitting and including the $^2\Pi_{3/2}$ and $^2\Pi_{1/2}$ spin-orbit states in the electronic partition function. It was assumed that spin-orbit coupling could be neglected in the pre-reaction adduct and in the saddle points.

2.2 Experimental Methods

European Photoreactor (EUPHORE). A series of experiments was carried out in chamber B of the EUPHORE facility in Valencia, Spain. The 200 m^3 polytetrafluoroethylene (PTFE) atmosphere simulation chamber has been described in detail elsewhere[38] and only the details pertinent to this work are given here. A syringe pump was used to inject known amounts of tBA (or d_9-tBA) into the chamber via a heated (120 °C) transfer line made of passivated stainless steel. The line was flushed with nitrogen during injection. Initial tBA mixing ratios in the EUPHORE chamber were ~220 ppbV. Nitric oxide (NO) was injected using a gas-tight syringe. A basic scrubber was inserted into the injection line for removing traces of nitric acid. Nitrogen dioxide (NO_2) was generated from NO via addition of ozone (O_3). The initial experimental conditions of the different experiments carried out are listed in the Supporting Experimental Information. After opening the chamber canopy, isopropyl nitrite (IPN) was continuously added to the chamber in a flow of nitrogen as an efficient OH radical precursor. Acetonitrile was used as a virtually inert dilution tracer in the kinetic study. The EUPHORE facility is equipped with standard monitors for pressure (p), temperature (T), relative humidity (RH), NO, NO_2, O_3, NO_2 photolysis frequency (j_{NO2}) and submicrometer particle size distribution. For the experiments described herein, we deployed a series of additional analyzers/analytical methods which are described in more detail in the following sections.

Proton-Transfer-Reaction Time-of-Flight Mass Spectrometry (PTR-ToF-MS). A commercial PTR-TOF 8000 instrument (Ionicon Analytik GmbH, Innsbruck, Austria) was used for measuring tBA and its photochemical oxidation products in the gas phase. The instrument has been described in detail elsewhere[39] and thus only the details pertinent to this study are described here. The drift tube was kept at a temperature of 100 °C and a pressure of 2.30 mbar. The electric field applied to the drift tube was periodically switched in 180 s intervals, i.e. measurements were performed at alternating E/N-values of 65 and 105 Td (1 Td = 10^{-17} V cm^{-2} $molecule^{-1}$), respectively. The PTR-TOF 8000 instrument was interfaced to the chamber using Siltek®/Sulfinert®-treated stainless steel tubing (total length: 143 cm, 60 cm

extending into the chamber, ID: 4.57 mm, temperature: 100 °C, flow: 20 lpm). The flow to the instrument was subsampled through PEEK® (polyetheretherketone) capillary tubing (OD: 1.59 mm). The instrument was regularly calibrated against a gaseous reference standard containing 13 hydrocarbons and oxygenated hydrocarbons. The instrument was further calibrated for tBA and tB-nitramine using a commercial liquid calibration unit (LCU; Ionicon Analytik GmbH, Innsbruck, Austria) for evaporation of gravimetrically prepared aqueous standards in nitrogen. For other analytes reported herein, we used theoretically derived instrumental response factors as listed in the Supporting Experimental Information.

Chemical Analysis of Aerosol Online (CHARON). A CHARON-PTR-ToF-MS instrument was used for measuring amines, amine degradation products and nitrate in the particulate phase. A prototype CHARON inlet[40,41] was interfaced to a second commercial PTR-TOF 8000 instrument (Ionicon Analytik GmbH, Innsbruck, Austria). The CHARON inlet strips off gas-phase analytes, enriches the particle concentration in the PTR-ToF-MS subsampling flow and vaporizes the particles prior to ionization and mass spectrometric analysis. In this study, the vaporization temperature was set to 140 °C. Vaporization occurs at an absolute pressure of a few mbar. The CHARON inlet was interfaced to the EUPHORE chamber using Siltek®/Sulfinert®-treated stainless steel tubing (total length: 415 cm, 40 cm extending into the chamber, ID: 4.57 mm). The PTR-ToF-MS drift tube was kept at a voltage of 350 V, a temperature of 130 °C and a pressure of 2.40 mbar (100 Td). The instrument was regularly calibrated against a gaseous reference standard containing 13 pure and oxygenated hydrocarbons. A reference mass spectrum was obtained from the tB-aminium nitrate salt.

Aerosol Mass Spectrometry [6]. A compact time-of-flight Aerosol Mass Spectrometer (C-ToF-AMS, Aerodyne Research Inc., Billerica, MA, U.S.A.)[42] was used for measuring total particle mass loading and particle chemical composition. A reference spectrum was obtained from the tB-aminium nitrate salt.

Thermosorb/N Cartridge Sampling and Analysis. Thermosorb/N cartridges (Cambridge Scientific Instruments Ltd., U.K.) were collected for detecting nitrosamines and nitramines. The cartridge was interfaced to the EUPHORE chamber using Siltek®/Sulfinert®-treated stainless steel tubing (total length: 50 cm, ID: 4.57 mm, kept at room temperature, sample gas flow: 1 lpm) with a stainless steel in-line particulate filter (pore size: 2 µm) and a stainless steel shut-off valve. A first cartridge was collected before addition of any reagents to the chamber (chamber background, 30 min sampling time). The second cartridge was collected after the addition of the amine precursor, before the chamber canopy had been opened (60 min sampling time). One or two additional cartridges were collected (60 min sampling time) after the chamber canopy had been opened. The cartridges were stored at -18 °C and sent to the laboratory where they were extracted and subjected to analysis using comprehensive two-dimensional Gas Chromatography - Nitrogen Chemiluminescence Detection (GC×GC-NCD). The details of the extraction process and chromatographic analysis are given in the Supporting Experimental Information. Recovery of *t*B-nitramine from the Thermosorb/N cartridges was determined by comparing the peak area obtained from a vapor spiked cartridge with the peak area obtained by direct standard injection. The recovery test was carried out in triplicate and an average recovery level of 61.5% was achieved (RSD <12%).

Quartz Filter Sampling and Analyses. At the end of each experiment, when the chamber canopy had been closed, the remaining aerosol was collected onto 47 mm diameter quartz fiber filters (Whatman, Maidstone, U.K.) using a high-volume sampling pump (flow rate: 48

lpm, sampling time: 60 min, total volume collected: 2.88 m^3). The filters had been pre-baked at 550 °C and wrapped in aluminum foil prior to sample collection. After collection, the samples were stored at -18 °C prior to analysis in the laboratory. Various extraction and chromatographic techniques were applied. GCx-GC-NCD was used for detecting nitrosamines and nitramines in the filter samples. Recovery of *t*B-nitramine from the filter paper was determined by comparing the peak area obtained from a spiked filter with the peak area obtained by direct standard injection. The recovery test was carried out in triplicate and an average recovery level of 86.6% was achieved (RSD = 3.52%). Comprehensive two-dimensional Gas Chromatography Time-of-Flight Mass Spectrometry (GC×GC-TOF-MS) was used for identifying additional amine photo-degradation products. Ion chromatography (IC) was used for determining the presence of tBA nitrate. Recovery of nitrate ($NaNO_3$) and tBA from the filter paper was determined by comparing the peak area obtained from a spiked filter with the peak area obtained by direct injection of the standards to the IC. The recovery tests were carried out in triplicate and average recovery levels of 98.8% (RSD = 0.3%) and 76.6% (RSD = 0.4%) were achieved for nitrate and tBA respectively. More details about the offline laboratory analyses are given in the Supporting Experimental Information.

Volatility Tandem Differential Mobility Analyzer (***VTDMA).*** A supplementary laboratory study was carried out to determine the thermal properties of the *tB*-aminium nitrate salt. The VTDMA used in these experiments has been described in detail previously[43,44] and specifically used for volatility studies on other alkyl aminium salts and ammonium nitrate (AN).[45] The thermal properties of aerosol particles were inferred from the rate of evaporation of submicrometer particles produced by nebulizing aqueous solutions of the tB-aminium nitrate salt. The particles were dried and a sample of narrow size distribution was selected using a differential mobility analyzer (DMA). A second DMA as part of an SMPS unit was used to determine the change in median diameter of the size distribution, resulting from evaporation in an oven unit set at selected temperatures between 298 and 393 K. Further details on the data analysis and the associated error are given in the Supporting Experimental Information and in the work by Salo et al.[45]

2.3 Chemicals

tBA (Sigma-Aldrich, ReagentPlus®, ≥99%), d_9-tBA (Sigma-Aldrich Chromasolv®, ≥99.9%), acetonitrile (Sigma-Aldrich, Chromasolv®, ≥99.8%), furan (Sigma-Aldrich, Chromasolv®, ≥99.8%) and *o*-xylene (Sigma-Aldrich, Chromasolv®, ≥99.9%) were used without further purification. 2-propyl nitrite (isopropyl nitrite, IPN) was synthesized from isopropanol, hydrochloric acid and sodium nitrite, and purified by repeated washing with ice water. tBA nitrate was prepared by adding an excess of diluted nitric acid (HNO_3) to diluted tBA followed by rotary evaporation to dryness at 80 °C.

Synthesis of tB-nitramine. *Warning: Handling of concentrated and fuming nitric acid (HNO_3) needs special precautions and safety equipment. Furthermore, all nitrated compounds should be treated as potential explosives.* Synthesis attempts based on a previously used method[46,47] failed (see Supporting Experimental Information). tB-nitramine was prepared modifying a previously published, low-yielding method.[48] By investigating the synthesis procedure, we concluded that the low yield was caused by the water solubility of the nitramine. In the original procedure, sufficient water to dissolve all the lithium salts was added, causing the nitramine to be lost during extraction. Consequently, the amount of

water added was reduced to a minimum followed by a more thorough extraction. This considerably improved the tB-nitramine yield. The detailed synthesis procedure was as follows. tBA (2.5 g, 34 mmol) was dissolved in 100 mL hexane and cooled to -78 °C under nitrogen. *n*-BuLi (2.6 M in hexane, 12 mL, 31 mmol) was added rapidly. The mixture was left stirring for 5 minutes, and ethyl nitrate[49] (1.46 g, 16 mmol) was added over the course of 1 hour. The reaction was left stirring for 1 hour at the same temperature when another portion of *n*-BuLi (5.8 mL, 15 mmol) was added, followed by ethyl nitrate (0.73 g, 8 mmol). After 30 minutes, the same addition of *n*-BuLi and ethyl nitrate was repeated. The reaction mixture was left stirring while being slowly heated to room temperature. Water (20 mL) was added to dissolve the lithium salts. The organic and aqueous layers were separated. The aqueous phase was cooled on an ice bath and acidified carefully to pH=1 with HCl_{aq} and extracted with ether (3x100 mL). The combined organic phases, including the hexane phase, was dried ($MgSO_4$), filtered and concentrated *in vacuo*. The crude product was distilled to give crystals of the target molecule (Bp: 86-87 ^{o}C (9 mmHg); Mp: 37-38 ^{o}C ; Yield: 1.8 g (51%)). All reagents and solvents were commercial grade and used without further purification.

3 RESULTS and DISCUSSION

3.1 Computational results

There are two possible routes in the reaction of tBA with OH radicals:

ΔH^{Θ} = -78 $(CH_3)_3CNH_2 + OH \rightarrow (CH_3)_2C(NH_2)\dot{C}H_2 + H_2O$ (1a)

ΔH^{Θ} = -70 $\rightarrow (CH_3)_3C\dot{N}H + H_2O$ (1b)

The reaction enthalpies (ΔH^{Θ}, in kJ mol^{-1}) stem from G4 calculations and refer to 298 K. Stationary points on the tBA + OH potential energy surface [50] were located in M06-2X and MP2 calculations employing the aug-cc-pVTZ basis set. Improved energies were obtained in CCSD(T*)-F12a/aug-cc-pVTZ computations. Six saddle points to the reaction were located, five to C-H and one to N-H abstraction. Figure 1 illustrates the relative energies of the stationary points on the PES based on MP2 structures.

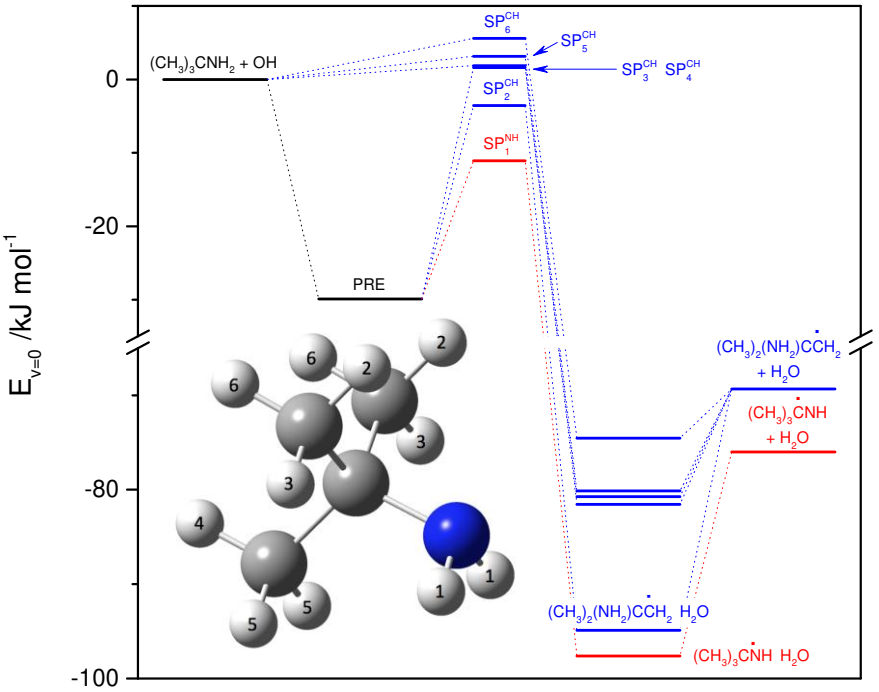

Figure 1. Stationary points on the PES of the tBA + OH reaction. Results from CCSD(T*)-F12a/aug-cc-pVTZ//MP2/aug-cc-pVTZ calculations.

Three of the five C-H abstraction routes proceed directly via low-barrier saddle points (SP_4^{CH} SP_6^{CH}), whereas two C-H abstractions (SP_2^{CH} and SP_3^{CH}) and the N-H abstraction (SP_1^{NH}) proceed via a common pre-reaction adduct (PRE). The subscripts increase with increasing saddle point energy and the H-atoms involved in the abstraction reactions are specified in Figure 1. All routes advance via post reaction complexes between the formed radicals and H_2O on the exit side. Energies, T_1[51] and D_1[52,53] diagnostics values, Cartesian coordinates and vibration-rotation data are provided in the Supporting Theoretical Information.

The MP2 and M06-2X results are virtually identical for the C-H abstraction routes while the results for N-H abstraction route differ significantly. The PES based on M06-2X structures is shown in the Supporting Theoretical Information along with the underlying quantum chemistry data. The most significant differences between the MP2 and M06-2X results lie in the saddle point structure and energy, and in the nature of the reaction coordinate. In the MP2 description, the N-H abstraction reaction is described as a "clean" H-transfer with an imaginary frequency of 1779 cm^{-1} and a saddle point energy $\Delta E_{v=0}$ ≈ -11 kJ mol^{-1}, whereas the N-H abstraction reaction is described with a significant –NH_2 torsional component, an imaginary frequency of only 405 cm^{-1} and a saddle point energy $\Delta E_{v=0}$ ≈ -6 kJ mol^{-1}, in the M06-2X calculations (see Supporting Theoretical Information). The other significant difference is the structure of the pre-reaction adduct(s) that were located in the IRC calculations. The MP2 calculations show a common, H-bonded pre-reaction adduct with the OH radical on the reaction coordinates to the C-H and N-H abstractions, in which the OH radical is H-bonded to the nitrogen lone-pair. The M06-2X IRC-calculations locate a pre-reaction adduct to N-H abstraction on a nearly flat surface in the vicinity of the saddle point SP_1^{NH}. Similar results have been reported for the OH reactions with methylamine[54] and piperazine.[50] We notice that the basis set superposition error (BSSE) in the M06-2X calculations of PRE_{NH}, estimated by the Counterpoise method,[55] is respectively 2.25 (aug-cc-

pVDZ) and 0.75 (aug-cc-pVTZ) kJ mol^{-1}. This is significant considering the flatness of the PES close to the saddle point leading to N-H abstraction. We also notice that the electronic energy difference between SP_1^{NH} and PRE_{NH} is 4.5 kJ mol^{-1} larger in the M06-2X/aug-cc-pVTZ calculation than the similar CCSD(T*)-F12a/aug-cc-pVTZ result, and conclude that the M06-2X localization of PRE_{NH} should be regarded with some skepticism.

Reaction (1) was investigated in a master equation model based on the PES illustrated in Figure 1. All vibrational modes were modelled as harmonic oscillators. The tBA + OH association reactions were treated as reversible reactions with rate coefficients approximated by typical values of $k_{association} = 4 \times 10^{-10} \times (T/298K)^{-1/6}$ cm^3 molecule^{-1} s^{-1} from long-range transition state theory.[56] The post-reaction adduct dissociations were also treated as reversible and approximated by the abovementioned rate coefficient for their formation reactions. The model results are essentially insensitive to variations in the Lennard–Jones parameters (ε and σ) and $<\Delta E_{down}>$, and only slightly sensitive to the value of the tBA + OH association rate coefficient: a 50% increase/decrease in $k_{association}$ resulted in a 3% increase, respectively 6% decrease in k_1 at 298 K. Figure 2 compares the calculated and experimental rate coefficients (see 3.2.1) for reaction (1). The branching in reaction (1) varies slightly with temperature: $k_{N\text{-}H}/k_{tot}$ ~0.99, ~0.96 and ~0.89 at respectively 200, 298 and 420 K in the MP2 structure based model, and ~0.84, ~0.80, and ~0.70 in the M06-2X structure based model. Modifying barrier heights can to a large extent counteract the difference between the calculated branching in the two models. However, the difference in predicted kinetic isotope effect (KIE) in the d_9-tBA + OH reaction cannot. The M06-2X based model predicts an essentially temperature independent KIE = $k_{d9\text{-}tBA+OH} / k_{tBA+OH}$ = 0.698 at 298 K, whereas the MP2 based model predicts an inverse kinetic isotope effect, KIE = 1.06 at 298 K. The experimental KIE is around 0.97 (see 3.2.1).

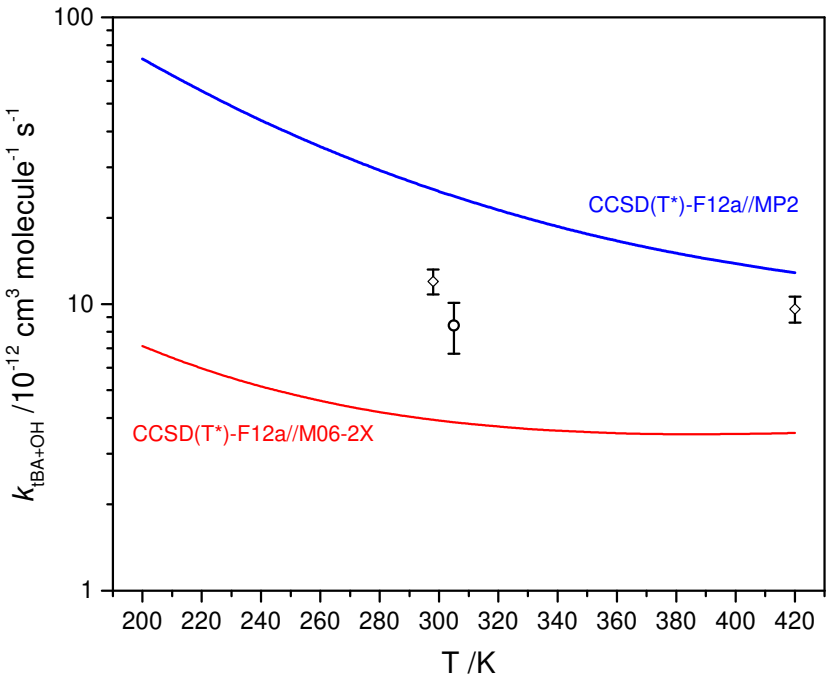

Figure 2. Observed and calculated rate coefficients for reaction (1) as a function of temperature. ○ This work; ◇ From Ref. 57

The theoretical study of the atmospheric fate of the $(CH_3)_2C(NH_2)\dot{C}H_2$ and $(CH_3)_3C\dot{N}H$ radicals is detailed in the Supporting Theoretical Information. The atmospheric reactions of these radicals are, with a single exception, shown to follow previously established routes.[7, 58] Here we focus on the exception which involves the transformation and decay of the primary nitrosamine ($(CH_3)_3CNHNO$, tB-nitrosamine) formed in the $(CH_3)_3C\dot{N}H$ + NO reaction:

$\Delta H^{\ominus}$ = -186 $(CH_3)_3C\dot{N}H + NO \rightarrow (CH_3)_3CNHNO^{\ddagger}$ (2)

$(CH_3)_3CNHNO \xrightarrow{h} (CH_3)_3C\dot{N}H + NO$ (3)

$\Delta H^{\ominus}$ = -14 $(CH_3)_3CNHNO^{\ddagger} \leftrightarrows (CH_3)_3CN{=}NOH^{\ddagger}$ (4)

$\Delta H^{\ominus}$ = -224 $(CH_3)_3CN{=}NOH\ddagger \rightarrow (CH_3)_2C{=}CH_2 + N_2 + H_2O$ (5)

The enthalpies are given in kJ mol^{-1}. The tB-nitrosamine exists in two conformations (*syn* or *anti* of the –HNNO moiety), whereas there are four stable conformations of the tB-hydroxydiazene (*syn-anti*, *syn-syn*, *anti-syn* and *anti-anti* of the CNNO and NNOH moieties). The barriers to rotational interconversion between the nitrosamine and hydroxydiazene conformers are well below the entrance energy of the reactants in (2). A simplified presentation of stationary points on the PES of reactions (2), (4) and (5) is given in Figure 3 (a complete description is given in the Supporting Theoretical Information).

The quantum chemistry calculations also reveal that the bond enthalpies of the N-H bond in $(CH_3)_3CNHNO$ and the O-H bond in $(CH_3)_3CN{=}NOH$ are only 332 and 345 kJ mol^{-1}, respectively. For comparison, the N-H and C-H bond enthalpies in tBA are 413 and 424 kJ mol^{-1}, respectively (G4 model chemistry). Both tB-nitrosamine and tB-hydroxydiazene are therefore expected to rapidly react with the OH radical:

$\Delta H^{\ominus}$ = -161 $(CH_3)_3CNHNO + OH \rightarrow (CH_3)_3CN{=}N\dot{O} + H_2O$ (6)

$\Delta H^{\ominus}$ = -147 $(CH_3)_3CN{=}NOH + OH \rightarrow (CH_3)_3CN{=}N\dot{O} + H_2O$ (7)

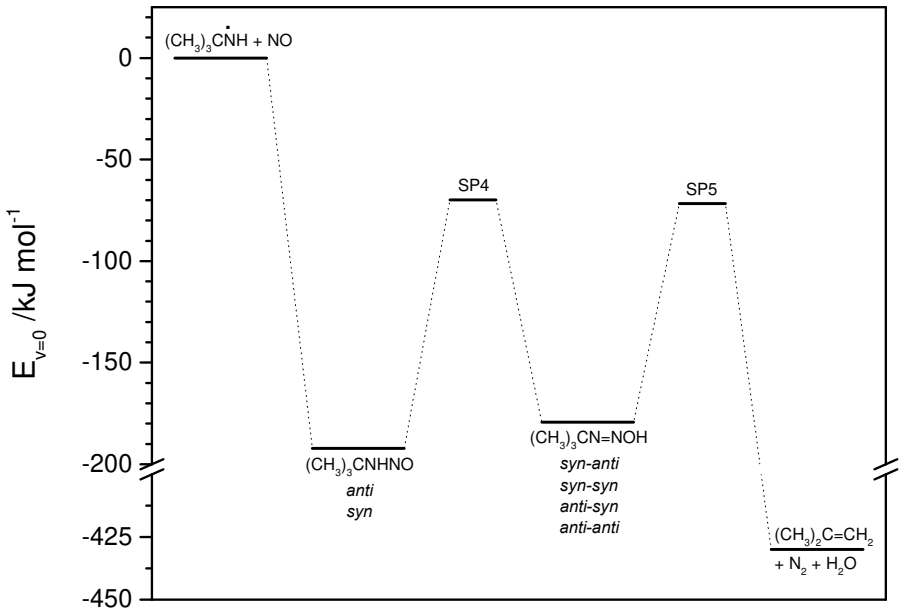

Figure 3. Stationary points on the simplified PES of the $(CH_3)_3C\dot{N}H$ + NO reaction. Results are from CCSD(T*)-F12a/aug-cc-pVTZ//M06-2X/aug-cc-pVTZ calculations.

The atmospheric fate of tB-nitrosamine was investigated in a master equation model based

on the PES illustrated in Figure 3 and including nitrosamine photolysis ($j_{Nitrosamine}$ = 0.34 × j_{NO2})[7] and the OH radical reactions (6) and (7). These reactions proceed via pre-reaction complexes and submerged barriers and have rate coefficients on the order of 10^{-10} cm^3 $molecule^{-1}$ s^{-1} (for more details see the Supporting Theoretical Information). For the chamber experiments conditions (<j_{NO2}> ~ 6 × 10^{-3} s^{-1}, <[OH]> ~ 10^7 cm^{-3}, see 3.2.1) the calculations suggest that ~75 % of the initially formed tB-nitrosamine is removed by the OH reactions (6) and (7), whereas ~25 % is removed by photolysis. Less than 1 % will be removed via reaction (5). For average ambient conditions (<j_{NO2}> ~ 1.6 × 10^{-3} s^{-1}, <[OH]> ~ 10^6 cm^{-3})[59] the calculations suggest that ~50 % of the initially formed nitrosamine is removed by the OH reactions (6) and (7), whereas ~45 % is removed by photolysis. Less than 5 % of the tB-nitrosamine will be removed via reaction (5). The $(CH_3)_3CN{=}N\dot{O}$ radical may subsequently dissociate resulting in the formation of nitrous oxide (N_2O). The barrier to dissociation of the $(CH_3)_3CN{=}N\dot{O}$ radical is ~ 50 kJ mol^{-1} below the entrance energy of the reactants and its atmospheric lifetime is consequently relatively short:

ΔH^{Θ} = +34 $\quad (CH_3)_3CN{=}N\dot{O} \rightarrow (CH_3)_3\dot{C} + NNO$ (8)

The atmospheric fate of $(CH_3)_3\dot{C}$ is well established and yields acetone and formaldehyde as the main products. The main routes in the atmospheric reactions of the $(CH_3)_3C\dot{N}H$ radical are summarized in Scheme 1. The main routes in the atmospheric reactions of the $(CH_3)_2C(NH_2)\dot{C}H_2$ radical are presented in the Supporting Theoretical Information.

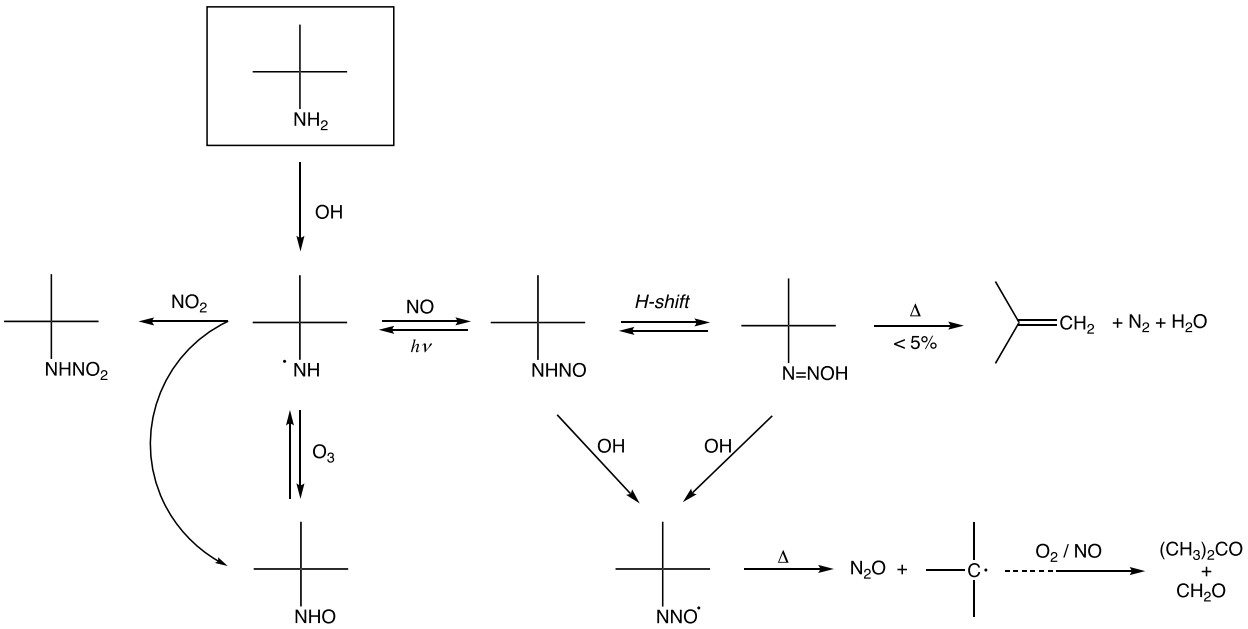

Scheme 1. Predicted atmospheric fate of the $(CH_3)_3C\dot{N}H$ radical.

3.2 Experimental results

3.2.1 OH reaction kinetics

We carried out two relative rate experiments in the EUPHORE chamber which included both tBA and d_9-tBA. Furan and *o*-xylene were used as reference compounds. Figure 4a displays the time evolution of the PTR-ToF-MS signal count rates as measured during the first kinetic

experiment. The second kinetic experiment is documented in the Supporting Experimental Information.

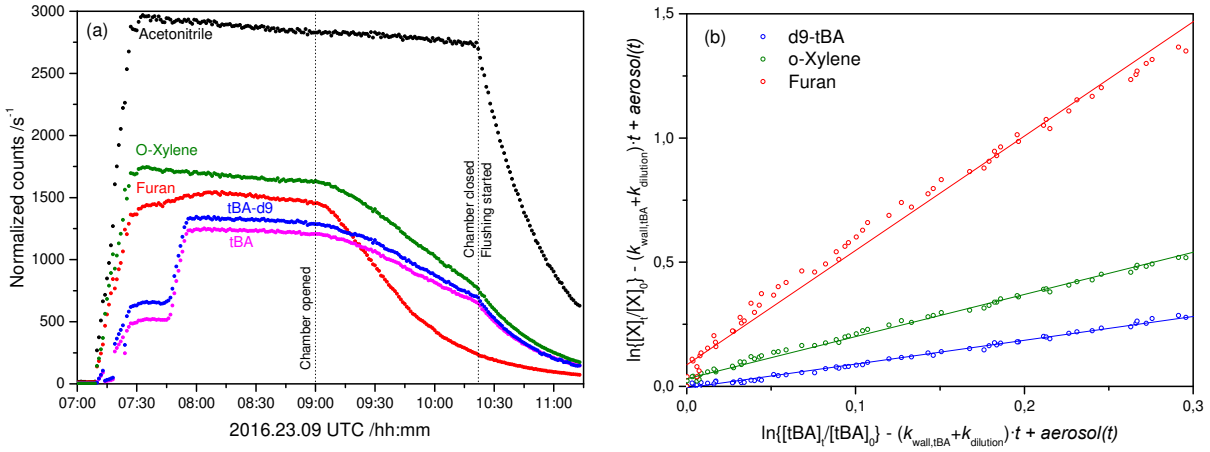

Figure 4. (a) Time evolution of tBA, d_9-tBA, the reference compounds o-xylene and furan, and the inert dilution tracer acetonitrile as observed during a relative rate experiment in the EUPHORE chamber. (b) Double-logarithmic plot showing the OH-induced decay of furan (black), o-xylene (red) and d_9-tBA (blue), respectively, relative to the decay of tBA. The data have been corrected for dilution losses and partitioning to the chamber walls and particles formed.

The dilution rates (derived from the decay of acetonitrile) in the two experiments were 6 and 9 × 10^{-6} s^{-1}, respectively. Wall loss rates (derived from the reagent decay prior to chamber opening) ranged from 1 to 2 × 10^{-5} s^{-1}. Initial mixing ratios were ~100 ppb for the reference compounds and ~200 ppb for tBA and d_9-tBA. Average OH densities in the EUPHORE chamber (derived from the reagent decay after chamber opening) were 9.1 × 10^6 cm^{-3} and 7.4 × 10^6 cm^{-3}, respectively. The average pressure in the two experiments was 1015 ± 1 mbar; average temperatures were 304 ± 2 K and 306 ± 2 K, respectively.

Least–squares fitting of the loss-corrected data (for details see Supporting Experimental Information) in Figure 4b resulted in the following relative rates (2σ statistical error limits): $k_{OH+tBA}/k_{OH+Furan}$ = 0.217 ± 0.005 and $k_{OH+tBA}/k_{OH+o\text{-}Xylene}$ = 0.589 ± 0.011. The duplicate experiment gave consistent results: $k_{OH+tBA}/k_{OH+Furan}$ = 0.205 ± 0.006, $k_{OH+tBA}/k_{OH+o\text{-}Xylene}$ = 0.567 ± 0.015. We suggest the averages as our best estimates for the relative rates: $k_{OH+tBA}/k_{OH+Furan}$ = 0.211 ± 0.006 and $k_{OH+tBA}/k_{OH+o\text{-}Xylene}$ = 0.578 ± 0.015. Using the currently recommended absolute rate coefficients at 305 K from critical reviews $k_{OH+Furan}$ = 3.95 × 10^{-11} (uncertainty factor 1.20)[60] and $k_{OH+o\text{-}Xylene}$ = 1.47 × 10^{-11} cm^3 $molecule^{-1}$ s^{-1} (uncertainty factor 1.25),[61] places our absolute values for k_{OH+tBA} at 8.3 ± 1.7 and 8.5 (± 2.1) × 10^{-12} cm^3 $molecule^{-1}$ s^{-1}, respectively. Assuming that there are no additional molecule specific systematic errors, we derive k_{OH+tBA} = 8.4 (± 1.7) × 10^{-12} cm^3 $molecule^{-1}$ s^{-1} at 305 ± 2 K and 1015 ± 1 hPa from the present experiments. For comparison, Koch et al.[57] reported k_{OH+tBA} = 1.20 (± 0.12) and 0.96 (± 0.10) × 10^{-11} cm^3 $molecule^{-1}$ s^{-1} at 298 and 420 ± 2 K, respectively, from flash photolysis/resonance fluorescence experiments. We note that neglecting the influence of particle formation in our experiments results in a rate coefficient of ~1.1 × 10^{-11} cm^3 $molecule^{-1}$ s^{-1}. An OH reaction rate coefficient of 8.4 x 10^{-12} cm^3 $molecule^{-1}$ s^{-1} results in an atmospheric lifetime of 33 hours assuming an averaged 24-hour OH radical number density of 1.0 x 10^6 molecules cm^{-3}.

The KIE ($k_{OH+d9\text{-}tBA}/k_{OH+tBA}$) measured in the two experiments was very small, 0.971 ± 0.011 and 0.968 ± 0.026, respectively. We take this as a first experimental evidence that the OH-initiated photo-oxidation of tBA is dominated by attack at the amino group.

3.2.2 Gas-phase products

Figures 5a and 5b show the PTR-ToF-MS mass spectra obtained from the gaseous products of the tBA + OH and the d_9-tBA + OH reaction, respectively. The reader is cautioned that the mass spectrum from the latter reaction also contains traces of non-deuterated products (carry-over effect). The time evolution of the reagent amine and the six main reaction products is plotted in Figure 5c. The product yield (on a carbon basis) is given in parentheses in the legend of Figure 5c. The yield was calculated for the first 50 minutes of reaction. Corrections for dilution losses and for partitioning of the amine to the chamber walls and particles have been applied.

The mass spectra show distinct signatures from the two main reaction products predicted by theory, acetone and tB-nitramine. *m/z* 59.049 ($C_3H_7O^+$) is the most abundant signal in both product mass spectra. We assign this peak to acetone which is, however, also the main product of IPN photolysis (used as OH radical precursor). The observation of deuterated acetone (*m/z* 65.087, $C_3D_6HO^+$) in Figure 5b confirms that acetone is also generated from the amine-OH reaction. Acetone (pink trace in Figure 5c) forms later than other species, confirming that it is a second-generation product.

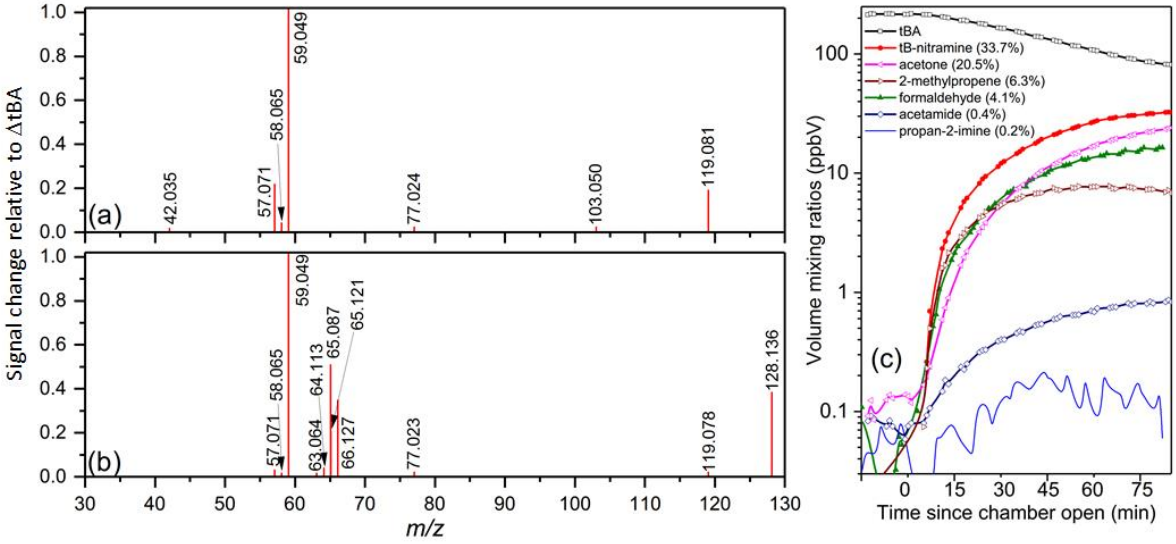

Figure 5. PTR-ToF-MS *mass spectra obtained from the gaseous products of the tBA + OH (a) and d_9-tBA + OH reaction (b). Only signals with a yield >1% ($\Delta cps_{product\ ion}/\Delta cps_{reagent\ ion}$) are shown. ^{13}C-isotopes and known chamber artefacts have been omitted. The time evolution of the reagent and major products (as observed during the d_9-tBA experiment) is shown in panel (c). The values in parentheses refer to the product yield (on a carbon basis) during the first 50 minutes of reaction.*

tB-nitramine was observed in high yields in its non-deuterated (*m/z* 119.083, $C_4H_{11}N_2O_2^+$) and deuterated (*m/z* 128.136, $C_4D_9H_2N_2O_2^+$) forms. We note that protonated tB-nitramine partially fragments to form the *tert*-butyl ion (*m/z* 57.070, $C_4H_9^+$, *m/z* 66.128 $C_4D_9^+$). Upon

calibration, tB-nitramine becomes the dominant reaction product (red trace in Figure 5c). The reported yield is a lower limit due to unaccounted losses of tB-nitramine to the chamber walls. tB-nitramine was also observed in the Thermosorb/N samples and the measurements were in good quantitative agreement with PTR-ToF-MS observations (for details see Supporting Experimental Information).

The product mass spectra also show the signatures of four minor products (formaldehyde, 2-methylpropene, acetamide and propan-2-imine) predicted by theory. The protonated formaldehyde peak is not shown in Figures 5a and 5b because the signal yield is smaller than 1%. Formaldehyde is, however, detected with reduced sensitivity in the PTR-ToF-MS instrument. Upon calibration, the small peak at *m/z* 33.030 (CD_2OH^+) becomes the third most abundant product of the tBA + OH reaction (green trace in Figure 5c). The *m/z* 65.121 peak ($C_4D_8H^+$) is assigned to 2-methylpropene (brown trace in Figure 5c). Acetamide cannot be detected in the experiment with the non-deuterated reagent due to a strong interference from ^{13}C-acetone. d_3-acetamide (*m/z* 63.063) is, however, seen in the mass spectrum obtained from the products of the d_9-tBA + OH reaction (Figure 5b). Propan-2-imine is detected in minor quantities at *m/z* 58.064 ($C_3H_8N^+$) and *m/z* 64.103 ($C_3D_6H_2N^+$), respectively. The time profile suggests a rapid loss of this species, either in the gas phase or via partitioning to the particle phase (see below).

Theory also predicts the formation of tB-nitrosamine, its isomer tB-hydroxydiazene and tB-hydroxylamine. We did not observe the *m/z*'s corresponding to the protonated molecules of these species. This may be owned to the fact that these compounds rapidly react with OH radicals, and that they are likely to dissociate upon protonation. We note that the predicted inorganic product, nitrous oxide (N_2O), cannot be detected by PTR-ToF-MS.

A few mass peaks in Figures 5a and 5b cannot be explained in terms of theoretically predicted degradation pathways of tBA. The peak at *m/z* 77.023 ($C_2H_5O_3^+$) is present in both mass spectra indicating that it is a by-product in IPN photolysis. The two minor peaks at *m/z* 42.035 ($C_2H_4N^+$) and *m/z* 103.049 ($C_3H_7N_2O_2^+$) are tentatively assigned to acetonitrile and CH_2=C(CH_3)$NHNO_2$, respectively. The latter probably generates from the photo-oxidation of the tB-nitramine.

3.2.3 Particle-phase products

In all experiments, the tBA + OH reaction was accompanied by strong particle formation (up to 10^5 #/cm^3) in the EUPHORE chamber (Figure 6a). AMS measurements indicate that the particles formed were mainly composed of tB-aminium nitrate (>90%, by mass), with the remaining fraction being made up of water and ammonium. IC analyses of the filter samples also found nitrate and the tB-aminium ion as the main ionic aerosol constituents (see Supporting Experimental Information). This finding does not come unexpected as all experiments were conducted in the presence of NO_x. Photochemically formed nitric acid is expected to react with the reagent amine (and other basic compounds in the chamber), forming low-volatility salts and thus inducing particle formation and growth.

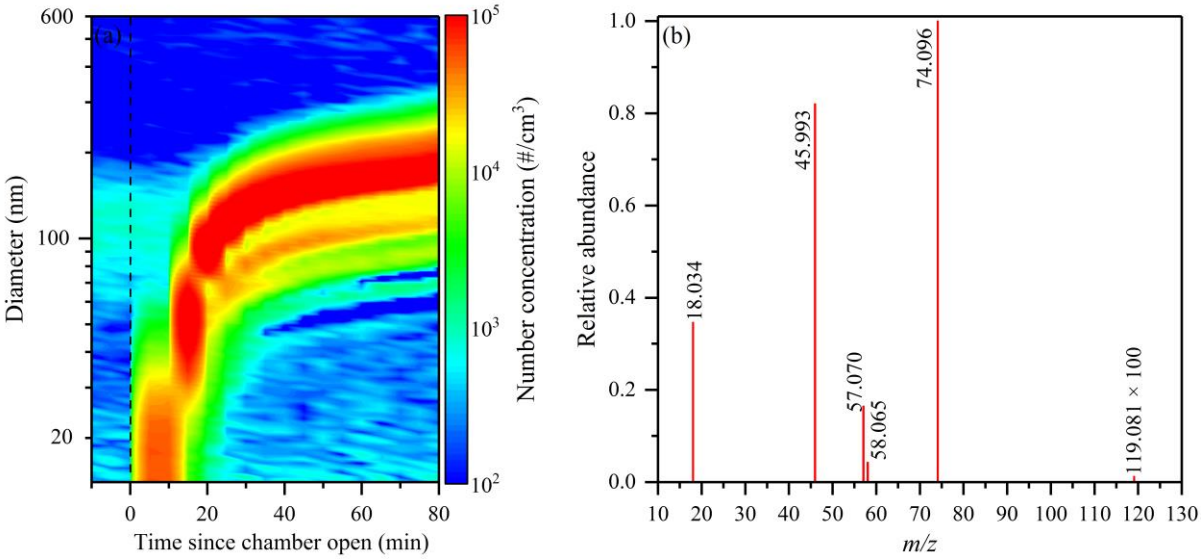

Figure 6. (a) Particle size distribution in the EUPHORE chamber as function of time (b) CHARON-PTR-ToF-MS mass spectrum obtained from the particles formed when tBA was reacted with OH radicals in the presence of NO_x.

The CHARON PTR-ToF-MS also observed tB-aminium nitrate in large abundances (Figure 6b). tBA is detected at *m/z* 18.033 (H_4N^+), 57.070 ($C_4H_9^+$) and 74.096 ($C_4H_{12}N^+$), while nitrate is detected at *m/z* 45.993 (NO_2^+). The minor peak at *m/z* 58.065 ($C_3H_8N^+$) is assigned to propan-2-imine. Our calculations indicate that the imine has an 8 kJ mol^{-1} higher proton affinity than the amine which makes it plausible that the imine displaces the amine in the salt. The protonated nitramine was only observed in traces (*m/z* 119.081 signal multiplied by 100 in Figure 6b; equivalent to concentrations in the low ng m^{-3} range). This contradicts our results from the filter samples onto which several hundreds of ng m^{-3} of tB-nitramine were detected (see Supporting Experimental Information). This may be explained by the adsorption of gaseous tB-nitramine onto the quartz filters. 2-methyl-2-nitropropane ($(CH_3)_3CNO_2$), N-*tert*-butylacetamide ($(CH_3)_3CNHC(O)CH_3$) and N-*tert*-butylformamide ($(CH_3)_3CNHC(O)H$) were also detected on the filter samples (see Supporting Experimental Information).

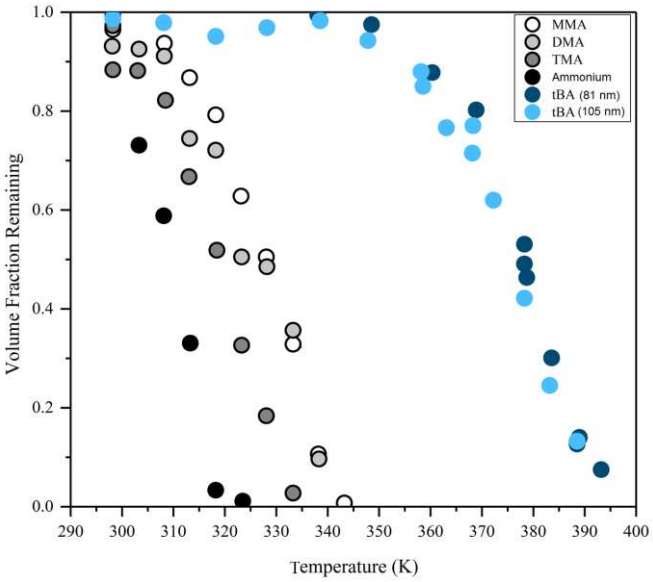

Figure 7. Thermal properties comparison of tB-aminium nitrate with corresponding nitrates from monomethylamine (MMA), dimethylamine (DMA) and trimethylamine (TMA). Data for ammonium nitrate have been included for reference. Two separate experiments with initial particle diameters of 81 and 105 nm, respectively, were carried out with tB-aminium nitrate particles.

The vapor pressure and enthalpy of vaporization of tB-aminium nitrate was determined in supplementary laboratory experiments. Figure 7 shows the volume fraction remaining when submicrometer particles composed of pure tB-aminium nitrate, methylaminium nitrate and dimethylaminium nitrate, respectively, were exposed to heat.

tB-aminium nitrate was found to be significantly less volatile than the alkylaminium nitrates. The vapor pressure of tB-aminium nitrate derived from the Clausius–Clapeyron relationship was 5.1 $\times 10^{-6}$ Pa at 298 K. The enthalpy of vaporization was determined to be 57 kJ mol^{-1}. It should be noted that we assumed evaporation of a liquid and not from a crystalline phase (for a detailed discussion see Salo et al.[45]). The low vapor pressure of tB-aminium nitrate explains the pronounced particle formation during the chamber experiments.

4 CONCLUSIONS

We have, for the first time, studied the reaction between OH radicals and an alkylamine in which the amino group is attached to a tertiary carbon. Hydrogen abstraction from the amino group was identified as the main reaction pathway. Our study confirms that potentially harmful nitramines are formed with high yield when amines are degraded in the atmosphere in the presence of NO_x. Any environmental impact assessment study will have to take into consideration the formation of nitramines and nitrosamines in the downwind region of an amine-based PCCC facility. While nitrosamines are generally assumed to rapidly photolyze in the atmosphere, in the case of the tB-nitrosamine a combination of isomerization to the corresponding hydroxydiazene and reaction with OH radicals were identified as competing pathways. We have demonstrated that the combined use of state-of-the art quantum chemical and online mass spectrometric methods for measuring gases

and aerosols (PTR-ToF-MS, CHARON-PTR-ToF-MS) is a powerful way to elucidate the kinetics and mechanism of the atmospheric breakdown of amines.

ASSOCIATED CONTENT

Supporting Experimental Information

Summary of experimental conditions of the photo-oxidation experiments. Collisional rate coefficients used for determining the PTR-ToF-MS response to non-calibrated compounds. Details on particle size distribution measurements, sample extraction and GC×GC-NCD, GC×GC-ToF-MS, ion chromatography analyses. Details of the VTDMA analyzer. Details on the failed synthesis of tB-nitramine. Details on the analysis of the kinetic experiments. Comparison of the tB-nitramine mixing ratios as measured by Thermosorb/N cartridges and by PTR-ToF-MS. Supplementary results from offline analyses of particle filters.

Supporting Theoretical Information

Tables with calculated (MP2 and M06-2X, respectively) electronic energies of reactants, intermediates and products of the $(CH_3)_3C(NH_2)$ + OH reaction. Detailed theoretical study on the atmospheric fate of the $(CH_3)_3C\dot{N}H$ and $(CH_3)_2C(NH_2)\dot{C}H_2$ radicals. Theoretical study on unimolecular fragmentation of selected protonated species. Tables of electronic energies of intermediates and products in the atmospheric photo-oxidation mechanism of tBA including T_1 and D_1 diagnostic values, vibrational frequencies rotational constants and Cartesian coordinates.

All Supporting Information is available free of charge via the Internet at http://pubs.acs.org

AUTHOR INFORMATION

Corresponding Author

*E-mail: armin.wisthaler@kjemi.uio.no. Phone: +47-22859139.

Notes

The authors declare no competing financial interest.

ACKNOWLEDGEMENTS

This work is part of the Atmospheric Chemistry of Amines (ACA) project supported by CLIMIT program under contract 244055, and has received additional support from the Research Council of Norway through a Centre of Excellence Grant (Grant No. 179568/V30). N. J. Farren acknowledges a NERC PhD studentship (NE/L501751/1). J. F. Hamilton acknowledges funding of the GCxGX-NCD instrument from NERC (NE/F01905X/1). The EUPHORE team is gratefully acknowledged for the support in the use of their facilities.

REFERENCES

1. Pitts, J. N.; Grosjean, D.; Van Cauwenberghe, K.; Schmid, J. P.; Fitz, D. R., Photooxidation of aliphatic amines under simulated atmospheric conditions: formation of nitrosamines, nitramines, amides, and photochemical oxidant. *Environmental Science & Technology* **1978,** *12* (8), 946-953.
2. Silva, E. F. d.; Hoff, K. A.; Booth, A., Emissions from CO_2 capture plants; an overview. *Energy Procedia* **2013,** *37*, 784-790.
3. Angelino, S.; Suess, D. T.; Prather, K. A., Formation of aerosol particles from reactions of secondary and tertiary alkylamines: Characterization by aerosol time-of-flight mass spectrometry. *Environmental Science & Technology* **2001,** *35* (15), 3130-3138.
4. Murphy, S.; Sorooshian, A.; Kroll, J.; Ng, N.; Chhabra, P.; Tong, C.; Surratt, J. D.; Knipping, E.; Flagan, R.; Seinfeld, J., Secondary aerosol formation from atmospheric reactions of aliphatic amines. *Atmospheric Chemistry and Physics* **2007,** *7* (9), 2313-2337.
5. Karl, M.; Dye, C.; Schmidbauer, N.; Wisthaler, A.; Mikoviny, T.; D'Anna, B.; Müller, M.; Borrás, E.; Clemente, E.; Muñoz, A., Study of OH-initiated degradation of 2-aminoethanol. *Atmospheric Chemistry and Physics* **2012,** *12* (4), 1881-1901.
6. Almeida, J.; Schobesberger, S.; Kurten, A.; Ortega, I. K.; Kupiainen-Maatta, O.; Praplan, A. P.; Adamov, A.; Amorim, A.; Bianchi, F.; Breitenlechner, M.; David, A.; Dommen, J.; Donahue, N. M.; Downard, A.; Dunne, E.; Duplissy, J.; Ehrhart, S.; Flagan, R. C.; Franchin, A.; Guida, R.; Hakala, J.; Hansel, A.; Heinritzi, M.; Henschel, H.; Jokinen, T.; Junninen, H.; Kajos, M.; Kangasluoma, J.; Keskinen, H.; Kupc, A.; Kurten, T.; Kvashin, A. N.; Laaksonen, A.; Lehtipalo, K.; Leiminger, M.; Leppa, J.; Loukonen, V.; Makhmutov, V.; Mathot, S.; McGrath, M. J.; Nieminen, T.; Olenius, T.; Onnela, A.; Petaja, T.; Riccobono, F.; Riipinen, I.; Rissanen, M.; Rondo, L.; Ruuskanen, T.; Santos, F. D.; Sarnela, N.; Schallhart, S.; Schnitzhofer, R.; Seinfeld, J. H.; Simon, M.; Sipila, M.; Stozhkov, Y.; Stratmann, F.; Tome, A.; Trostl, J.; Tsagkogeorgas, G.; Vaattovaara, P.; Viisanen, Y.; Virtanen, A.; Vrtala, A.; Wagner, P. E.; Weingartner, E.; Wex, H.; Williamson, C.; Wimmer, D.; Ye, P.; Yli-Juuti, T.; Carslaw, K. S.; Kulmala, M.; Curtius, J.; Baltensperger, U.; Worsnop, D. R.; Vehkamaki, H.; Kirkby, J., Molecular understanding of sulphuric acid-amine particle nucleation in the atmosphere. *Nature* **2013,** *502* (7471), 359-363.
7. Nielsen, C. J.; Herrmann, H.; Weller, C., Atmospheric chemistry and environmental impact of the use of amines in carbon capture and storage (CCS). *Chemical Society Reviews* **2012,** *41* (19), 6684-6704.
8. Wagner, E. D.; Osiol, J.; Mitch, W. A.; Plewa, M. J., Comparative in vitro toxicity of nitrosamines and nitramines associated with amine-based carbon capture and storage. *Environmental Science & Technology* **2014,** *48* (14), 8203-8211.
9. Låg, M.; Lindeman, B.; Instanes, C.; Brunborg, G.; Schwarze, P., Health effects of amines and derivatives associated with CO_2 capture. *IARC Sci Publ* **2011**, 57.
10. Bråten, H.; Bunkan, A.; Bache-Andreassen, L.; Solimannejad, M.; Nielsen, C., Final report on a theoretical study on the atmospheric degradation of selected amines. *Report: NILU: OR* **2008,** *77*.
11. Nielsen, C.; D'Anna, B.; Bossi, R.; Bunkan, A.; Dithmer, L.; Glasius, M.; Hallquist, M.; Hansen, A.; Lutz, A.; Salo, K., Atmospheric degradation of amines (ADA), *summary report: gas phase photo-oxidation of 2-aminoethanol (MEA)* **2010**.
12. Onel, L.; Blitz, M.; Breen, J.; Rickard, A.; Seakins, P., Branching ratios for the reactions of OH with ethanol amines used in carbon capture and the potential impact on carcinogen formation in the emission plume from a carbon capture plant. *Physical Chemistry Chemical Physics* **2015,** *17* (38), 25342-25353.
13. Luis, P., Use of monoethanolamine (MEA) for CO_2 capture in a global scenario: consequences and alternatives. *Desalination* **2016,** *380*, 93-99.
14. Bougie, F.; Iliuta, M. C., Sterically hindered amine-based absorbents for the removal of CO_2 from gas streams. *Journal of Chemical & Engineering Data* **2012,** *57* (3), 635-669.

15. Davis, J. D., Thermal degradation of aqueous amines used for carbon dioxide capture. *The University of Texas at Austin, Ph.D. Dissertation* **2009**.
16. Eide-Haugmo, I.; Lepaumier, H.; da Silva, E. F.; Einbu, A.; Vernstad, K.; Svendsen, H. F. In *A study of thermal degradation of different amines and their resulting degradation products*, 1st Post Combustion Capture Conference, IEA Greenhouse Gas R&D Programme, Abu Dhabi, United Arab Emirates, 2011; pp 17-19.
17. Wang, T.; Jens, K.-J., Oxidative degradation of aqueous 2-amino-2-methyl-1-propanol solvent for postcombustion CO_2 capture. *Industrial & Engineering Chemistry Research* **2012,** *51* (18), 6529-6536.
18. Wang, T., Degradation of aqueous 2-Amino-2-methyl-1-propanol for carbon dioxide capture. *Telemark University College, Ph.D. Dissertation* **2013**.
19. Zhao, Y.; Truhlar, D. G., The M06 suite of density functionals for main group thermochemistry, thermochemical kinetics, noncovalent interactions, excited states, and transition elements: two new functionals and systematic testing of four M06-class functionals and 12 other functionals. *Theoretical Chemistry Accounts: Theory, Computation, and Modeling (Theoretica Chimica Acta)* **2008,** *120* (1), 215-241.
20. Møller, C.; Plesset, M. S., Note on an approximation treatment for many-electron systems. *Physical Review* **1934,** *46* (7), 618-622.
21. Dunning Jr, T. H., Gaussian basis sets for use in correlated molecular calculations. I. The atoms boron through neon and hydrogen. *The Journal of chemical physics* **1989,** *90* (2), 1007-1023.
22. Kendall, R. A.; Dunning Jr, T. H.; Harrison, R. J., Electron affinities of the first - row atoms revisited. Systematic basis sets and wave functions. *The Journal of Chemical Physics* **1992,** *96* (9), 6796-6806.
23. Hratchian, H. P.; Schlegel, H. B., Accurate reaction paths using a Hessian based predictor–corrector integrator. *The Journal of Chemical Physics* **2004,** *120* (21), 9918-9924.
24. Hratchian, H. P.; Schlegel, H. B., *Theory and Applications of Computational Chemistry: The First 40 Years*. Elsevier: Amsterdam, 2005.
25. Hratchian, H. P.; Schlegel, H. B., Using Hessian updating to increase theefficiency of a Hessian based predictor-corrector reaction path following method. *Journal of Chemical Theory and Computation* **2005,** *1* (1), 61-69.
26. Adler, T. B.; Knizia, G.; Werner, H.-J., A simple and efficient CCSD (T)-F12 approximation. AIP: 2007.
27. Knizia, G.; Adler, T. B.; Werner, H.-J., Simplified CCSD (T)-F12 methods: theory and benchmarks. *The Journal of Chemical Physics* **2009,** *130* (5), 054104.
28. Curtiss, L. A.; Redfern, P. C.; Raghavachari, K., Gaussian-4 theory. *The Journal of Chemical Physics* **2007,** *126* (8), 084108.
29. Su, T., Parametrization of kinetic energy dependences of ion–polar molecule collision rate constants by trajectory calculations. *The Journal of Chemical Physics* **1994,** *100* (6), 4703-4703.
30. Werner, H.; Knowles, P.; Knizia, G.; Manby, F.; Schütz, M.; Celani, P.; Korona, T.; Lindh, R.; Mitrushenkov, A.; Rauhut, G., MOLPRO, version 2012.1, a package of ab initio programs. *Search PubMed* **2012**.
31. Werner, H.-J.; Knowles, P. J.; Knizia, G.; Manby, F. R.; Schütz, M., Molpro: a general-purpose quantum chemistry program package. *Wiley Interdisciplinary Reviews: Computational Molecular Science* **2012,** *2* (2), 242-253.
32. Frisch, M.; Trucks, G.; Schlegel, H.; Scuseria, G.; Robb, M.; Cheeseman, J.; Scalmani, G.; Barone, V.; Mennucci, B.; Petersson, G.; Nakatsuji, H.; Caricato, M.; Li, X.; Hratchian, H. P.; Izmaylov, A. F.; Bloino, J.; Zheng, G.; Sonnenberg, J. L.; Hada, M.; Ehara, M.; Toyota, K.; Fukuda, R.; Hasegawa, J.; Ishida, M.; Nakajima, T.; Honda, Y.; Kitao, O.; Nakai, H. V., T.; Montgomery, J., J. A.; Peralta, J. E. O., F.; Bearpark, M. H., J. J.; Brothers, E. K., K. N.; Staroverov, V. N.; Kobayashi, R.; Normand, J.; Raghavachari, K.; Rendell, A.; Burant, J. C.; Iyengar, S. S.; Tomasi, J.; Cossi, M.; Rega, N.; Millam, J. M.; Klene, M.; Knox, J. E.; Cross, J. B.; Bakken, V.; Adamo, C.; Jaramillo, J.; Gomperts, R.; Stratmann, R. E.;

Yazyev, O.; Austin, A. J.; Cammi, R.; Pomelli, C.; Ochterski, J. W.; Martin, R. L.; Morokuma, K.; Zakrzewski, V. G.; Voth, G. A.; Salvador, P.; Dannenberg, J. J.; Dapprich, S.; Daniels, A. D.; Farkas, Ö.; Foresman, J. B.; Ortiz, J. V.; Cioslowski, J.; Fox, D. J., Gaussian 09, Revision A. 02. Gaussian Inc., Wallingford, CT. **2009**.

33. Glowacki, D. R.; Liang, C.-H.; Morley, C.; Pilling, M. J.; Robertson, S. H., MESMER: an open-source master equation solver for multi-energy well reactions. *The Journal of Physical Chemistry A* **2012,** *116* (38), 9545-9560.

34. Bartis, J. T.; Widom, B., Stochastic models of the interconversion of three or more chemical species. *The Journal of Chemical Physics* **1974,** *60* (9), 3474-3482.

35. Miller, J. A.; Klippenstein, S. J., Master equation methods in gas phase chemical kinetics. *The Journal of Physical Chemistry A* **2006,** *110* (36), 10528-10544.

36. Mourits, F. M.; Rummens, F. H., A critical evaluation of Lennard–Jones and Stockmayer potential parameters and of some correlation methods. *Canadian Journal of Chemistry* **1977,** *55* (16), 3007-3020.

37. Coxon, J.; Foster, S., Radial dependence of spin-orbit and Λ-doubling parameters in the X2Π ground state of hydroxyl. *Journal of Molecular Spectroscopy* **1982,** *91* (1), 243-254.

38. Becker, K. H., *The European photoreactor EUPHORE: design and technical development of the European photoreactor and first experimental results: final report of the EC-project: contract EV5V-CT92-0059: Funding Period, January 1993-December 1995*. 1996.

39. Jordan, A.; Haidacher, S.; Hanel, G.; Hartungen, E.; Märk, L.; Seehauser, H.; Schottkowsky, R.; Sulzer, P.; Märk, T. D., A high resolution and high sensitivity proton-transfer-reaction time-of-flight mass spectrometer (PTR-TOF-MS). *International Journal of Mass Spectrometry* **2009,** *286* (2–3), 122-128.

40. Eichler, P.; Muller, M.; D'Anna, B.; Wisthaler, A., A novel inlet system for online chemical analysis of semi-volatile submicron particulate matter. *Atmospheric Measurement Techniques* **2015,** *8* (3), 1353-1360.

41. Eichler, P.; Müller, M.; Rohmann, C.; Stengel, B.; Orasche, J. ; Zimmermann, R.; Wisthaler, A., Lubricating Oil as a major constituent of ship exhaust particles. *Environmental Science & Technology Letters* **2017,** *4* (2), 54-58.

42. Drewnick, F.; Hings, S. S.; DeCarlo, P.; Jayne, J. T.; Gonin, M.; Fuhrer, K.; Weimer, S.; Jimenez, J. L.; Demerjian, K. L.; Borrmann, S., A new time-of-flight aerosol mass spectrometer (TOF-AMS)—Instrument description and first field deployment. *Aerosol Science and Technology* **2005,** *39* (7), 637-658.

43. Jonsson, Å. M.; Hallquist, M.; Saathoff, H., Volatility of secondary organic aerosols from the ozone initiated oxidation of α-pinene and limonene. *Journal of Aerosol Science* **2007,** *38* (8), 843-852.

44. Salo, K.; Jonsson, Å. M.; Andersson, P. U.; Hallquist, M., Aerosol volatility and enthalpy of sublimation of carboxylic acids. *The Journal of Physical Chemistry A* **2010,** *114* (13), 4586-4594.

45. Salo, K.; Westerlund, J.; Andersson, P. U.; Nielsen, C. J.; D'Anna, B.; Hallquist, M., Thermal characterization of aminium nitrate nanoparticles. *The Journal of Physical Chemistry A* **2011,** *115* (42), 11671-11677.

46. Maguta, M. M.; Aursnes, M.; Bunkan, A. J. C.; Edelen, K.; Mikoviny, T.; Nielsen, C. J.; Stenstrøm, Y.; Tang, Y.; Wisthaler, A., Atmospheric fate of nitramines: An experimental and theoretical study of the OH reactions with CH_3NHNO_2 and $(CH_3)_2NNO_2$. *The Journal of Physical Chemistry A* **2014,** *118* (19), 3450-3462.

47. Antonsen, S.; Aursnes, M.; Gallantree-Smith, H.; Dye, C.; Stenstrøm, Y., Safe synthesis of alkylhydroxy and alkylamino nitramines. *Molecules* **2016,** *21* (12), 1738.

48. Winters, L. J.; Learn, D. B.; Desai, S. C., A Preparation of primary aliphatic nitramines. *The Journal of Organic Chemistry* **1965,** *30* (7), 2471-2472.

49. Higgins, C. M.; Evans, L. A.; Lloyd-Jones, G. C.; Shallcross, D. E.; Tew, D. P.; Orr-Ewing, A. J., Quantum yields for photochemical production of NO_2 from organic nitrates at tropospherically relevant wavelengths. *The Journal of Physical Chemistry A* **2014,** *118* (15), 2756-2764.

50. Sarma, P. J.; Gour, N. K.; Bhattacharjee, D.; Mishra, B. K.; Deka, R. C., Hydrogen atom abstraction from Piperazine by hydroxyl radical: a theoretical investigation. *Molecular Physics* **2017,** *115* (8), 962-970.
51. Lee, T. J.; Taylor, P. R., A diagnostic for determining the quality of single‐reference electron correlation methods. *International Journal of Quantum Chemistry* **1989,** *36* (S23), 199-207.
52. Janssen, C. L.; Nielsen, I. M., New diagnostics for coupled-cluster and Møller–Plesset perturbation theory. *Chemical physics letters* **1998,** *290* (4), 423-430.
53. Lee, T. J., Comparison of the T 1 and D 1 diagnostics for electronic structure theory: a new definition for the open-shell D 1 diagnostic. *Chemical physics letters* **2003,** *372* (3), 362-367.
54. Borduas, N.; Abbatt, J. P. D.; Murphy, J. G.; So, S.; da Silva, G., Gas-phase mechanisms of the reactions of reduced organic nitrogen compounds with OH radicals. *Environmental Science & Technology* **2016,** *50* (21), 11723-11734.
55. Boys, S. F.; Bernardi, F., The calculation of small molecular interactions by the differences of separate total energies. Some procedures with reduced errors. *Molecular Physics* **1970,** *19* (4), 553-566.
56. Georgievskii, Y.; Klippenstein, S. J., Long-range transition state theory. *The Journal of chemical physics* **2005,** *122* (19), 194103.
57. Koch, R.; Kruger, H. U.; Elend, M.; Palm, W. U.; Zetzsch, C., Rate constants for the gas-phase reaction of OH with amines: tert-Butyl amine, 2,2,2-trifluoroethyl amine, and 1,4-diazabicyclo[2.2.2]octane. *International Journal of Chemical Kinetics* **1996,** *28* (11), 807-815.
58. Onel, L.; Thonger, L.; Blitz, M. A.; Seakins, P. W.; Bunkan, A. J. C.; Solimannejad, M.; Nielsen , C. J., Gas phase reactions of OH with methyl amines in the presence or absence of molecular oxygen. An experimental and theoretical study. *J. Phys. Chem. A* **2013,** *117* (41), 10736-10745.
59. Wolke, R.; Schröder, W.; Schrödner, R.; Renner, E., Influence of grid resolution and meteorological forcing on simulated European air quality: A sensitivity study with the modeling system COSMO–MUSCAT. *Atmospheric Environment* **2012,** *53* (Supplement C), 110-130.
60. Atkinson, R.; Baulch, D. L.; Cox, R. A.; Crowley, J. N.; Hampson, R. F.; Hynes, R. G.; Jenkin, M. E.; Rossi, M. J.; Troe, J., Evaluated kinetic and photochemical data for atmospheric chemistry: Volume II - gas phase reactions of organic species. *Atmospheric Chemistry and Physics* **2006,** *6*, 3625-4055.
61. Atkinson, R., Kinetics and mechanisms of the gas-phase reactions of the hydroxyl radical with organic compounds under atmospheric conditions. *Chemical Reviews* **1986,** *86* (1), 69-201.

TOC Graphic